

Size estimates for intervening C IV absorbers from high resolution spectroscopy of APM 0827+5255.

Panayiotis Tzanavaris[★], Robert F. Carswell[†]

Institute of Astronomy, Cambridge CB3 0HA

Accepted Received;

ABSTRACT

A new analysis of Keck/HIRES observations of the broad absorption line QSO APM 0827+5255 indicates that a number of intervening C IV absorbers give rise to absorption lines for which the observed optical depths for 1548, 1550 Å doublet components are not in the expected 2 : 1 ratio. To compensate for the effect, a local adjustment of the zero-level is required. We model this effect as coverage of one line of sight to this gravitationally lensed QSO and perform a set of simulations to select a sample of lines for which our model provides an explanation for the effect. We use lines in this sample to obtain estimates for minimum C IV absorber sizes from total coverage and the separations of the lines of sight for a range of lens redshifts, z_1 , and two cosmologies. We also obtain best estimates for overall sizes from a statistical ‘hit and miss’ approach. For $z_1 = 0.7$ our results set a lower limit to sizes of C IV absorbers of $\sim 0.3 h_{72}^{-1}$ kpc ($\sim 0.5 h_{72}^{-1}$ kpc) for $\Omega_M = 1, \Omega_\Lambda = 0$ ($\Omega_M = 0.3, \Omega_\Lambda = 0.7$), in agreement with other results from similar work but are limited by sample size and the uncertainty in z_1 . Our method can be used to detect lensed QSOs and to probe absorber sizes when separate spectra cannot be obtained for each line of sight.

Key words: cosmology: observations – gravitational lensing – intergalactic medium – methods: miscellaneous – quasars: absorption lines – quasars: individual (APM 0827+5255)

1 INTRODUCTION

The advent of 10-m class telescopes in the last decade has provided us with an unprecedented view of the high-redshift universe. In particular, HIRES, the high-resolution echelle spectrograph on the Keck I telescope in Hawaii, has made it possible to obtain observations with resolution as high as $\sim 6 \text{ km s}^{-1}$. As a result, a number of detailed studies of absorption lines in the spectra of background QSOs have been carried out (for reviews see Rauch 1998; Hamann & Ferland 1999).

However, this improvement in *spectral* resolution cannot be easily accompanied by an improvement in *spatial* resolution: 2-dimensional information about the absorbers can normally only be obtained by comparing separate spectra of multiple quasar images, which are due to either gravitationally lensed single QSOs or actual QSO pairs which have a small angular separation on the plane of the sky. Because lensed QSOs have image separations up to a few arcseconds, they are useful for probing scales $\lesssim 100$ kpc. QSO pairs have

image separations of at least a few arcminutes, thus allowing one to probe scales of a few hundred kpc. From coincident absorption in more than one line of sight (LOS), minimum size (coherence length) estimates can be obtained immediately. Estimates of most probable sizes require a statistical ‘hit and miss’ approach (e.g. McGill 1990).

Such studies have led to size estimates for Lyman α absorbers ranging from a few kpc (Foltz et al. 1984; McGuill 1990; Bechtold & Yee 1995) to a few hundred kpc (Dinshaw et al. 1995; Smette et al. 1995; Dinshaw et al. 1998) to ~ 1 Mpc (Fang et al. 1996; Dinshaw et al. 1997; Young et al. 2001). Such large ‘sizes’ suggest that the typical, low column density ($\lesssim 10^{14.5} \text{ cm}^{-2}$) Lyman α forest line does not originate in discrete galactic or protogalactic clouds. The emerging picture is consistent with results from hydrodynamical numerical simulations in a Cold Dark Matter (CDM) structure formation scenario according to which the Lyman α forest is a manifestation of a space filling photoionized intergalactic medium (IGM). This is the most important baryon reservoir in the Universe at high redshift (see e.g. Efstathiou, Schaye & Theuns 2000 for a review).

The C IV doublet ($\lambda\lambda 1548.20, 1550.78 \text{ \AA}$) is the most commonly observed heavy-element absorption signature red-

[★] e-mail: pt2@ast.cam.ac.uk

[†] e-mail: rfc@ast.cam.ac.uk

ward of the Lyman α emission line in spectra of high-redshift QSOs. The oscillator strengths for the 1548.20 and 1550.78 Å components are in a 2 : 1 ratio, which translates to the same optical depth ratio for optically thin ($\tau \ll 1$) lines.

Line parameters are consistent with a photoionized gas (Rauch et al. 1996). The C IV absorbers appear to be highly clustered (Sargent et al. 1988; Petitjean & Bergeron 1994; Loh, Quashnock & Stein 2001) and have been thought to originate in gas clouds orbiting in galactic haloes (Sargent et al. 1979; Steidel 1993; Petitjean & Bergeron 1994; Mo & Miralda-Escudé 1996). Hydrodynamical simulations also support a picture in which high-redshift C IV arises in protogalactic clumps (PGCs), i.e., small, future constituents of large galaxies, forming through gravitational instability in a hierarchical cosmogony (Haehnelt, Steinmetz & Rauch 1996; Rauch, Haehnelt & Steinmetz 1997).

Size estimates for heavy element absorbers range from a few kpc (Young et al. 1981; Smette et al. 1992; Monier, Turnshek & Lupie 1998) to a few tens of kpc (Crotts et al. 1994; Smette et al. 1995; Lopez, Hagen & Reimers 2000) or even hundreds of kpc (Shaver & Robertson 1983; Petitjean et al. 1998). A recent study using three gravitationally lensed QSOs (Rauch, Sargent & Barlow 2001) obtains size estimates on the order of kiloparsecs. It is also apparent that sizes are absorber-type dependent, with individual clouds for low-ionization absorbers having dimensions on the order of a few $\times 10$ pc as opposed to at least a few $\times 100$ pc for high-ionization absorbers (Rauch, Sargent & Barlow 1999; Rauch et al. 2001; Rigby, Charlton & Churchill 2002).

With an *R*-band magnitude of 15.2 (Irwin et al. 1998) APM 0827+5255 is one of the intrinsically most luminous QSOs known (bolometric luminosity $\lesssim 10^{15} L_{\odot}$, Egami et al. 2000; Ibata et al. 1999). From molecular CO emission lines the estimated quasar redshift is $z = 3.911$ (Downes et al. 1999). It is thus well suited for QSO absorption line studies. Additionally, the object is gravitationally lensed (Ledoux et al. 1998; Ibata et al. 1999; Egami et al. 2000) but the redshift of the lens is not known. As the object is lensed into three images, it represents the first confirmed odd-image lens system (Lewis et al. 2002).

For this object it is not possible to obtain separate spectra for different LOS with ground-based observations (image separation ~ 0.38 arcsec). However, if only one LOS is covered, there is an excess in the continuum intensity that gets through to the observer. If the absorbing column is high enough, the observed optical depths of the components of a heavy element doublet are not in the expected ratio, providing a signature for this effect. We use the term Anomalous Doublet Ratio (ADR) for such doublets. In such a case, in order to obtain a satisfactory fit, one has to adjust the spectral zero level locally. A number of Mg II systems show this effect in APM 0827+5255. By means of equivalent width modelling Petitjean et al. (2000) have obtained size estimates of ~ 1 kpc for Mg II cloudlets. From separate near-infrared spectra for each LOS Kobayashi et al. (2002) obtain upper limit estimates of ~ 200 pc for Mg II clouds in a damped Lyman α system.

We have used the ADR to select lines from intervening C IV systems which may be due to coverage of one LOS towards APM 0827+5255. The observations and data reduction are described in Section 2, the fitting procedure in

Section 3 and our partial coverage model in Section 4. We have run a set of simulations to establish whether the effect can be genuine for each fitted line, and these are described in Section 5. We have then used a maximum likelihood analysis to obtain estimates for the most probable sizes of the C IV absorbers (Section 6). We have used the currently favoured cosmological model with matter density $\Omega_M = 0.3$, and vacuum energy density $\Omega_{\Lambda} = 0.7$ (Perlmutter et al. 1999; Riess et al. 1998; Riess et al. 2001). To facilitate comparisons with previous work, where $q_0 = 0.5$ ($\Omega_M = 1, \Omega_{\Lambda} = 0$) is used almost exclusively, we have also carried out the calculations for such a model. $H_0 = 72 h_{72} \text{ km s}^{-1} \text{ Mpc}^{-1}$ (Freedman et al. 2001) throughout. We discuss our results in Section 7 and conclude in Section 8.

2 OBSERVATIONS AND DATA REDUCTION

The data used in this analysis were obtained through a programme of high resolution observations on the 10-m Keck I telescope in Hawaii in April and May 1998 using HIRES with the TeK 2048 \times 2048 CCD at the Nasmyth focus. Details of the observations can be found in Ellison et al. (1999b). The data have been made publicly available (Ellison et al. 1999a) but we did not use the version available on the internet because there are a number of discontinuities due to inappropriate merging of the orders (also noticed by Petitjean et al. 2000). Instead, we used the original data files. However, in two of the exposures there was a spurious systematic shift in wavelength of ~ 0.2 Å, due to incorrect dating and, hence, incorrect heliocentric velocity correction. After correcting for this problem, we used Tom Barlow's MAuna Kea Echelle Extraction programme (see <http://www2.keck.hawaii.edu:3636/realpublic/inst/hires/makeewww/index.html>) to obtain a set of disjoint echelle orders, wavelength calibrated and rebinned onto a linear wavelength scale of 0.04 Å per pixel.

We have flux calibrated each echelle order individually by means of the available standard stars and standard IRAF routines to ensure that there were no discontinuities where they were joined. The orders were joined by means of specially written interactive IRAF scripts which ensured a smooth joining of adjacent and overlapping parts with weights proportional to the local signal-to-noise ratio (SNR). A continuous spectrum has thus been formed for which the continuum does not change abruptly. This continuum was fitted using cubic spline functions in spectral regions deemed free of absorption.

3 ABSORPTION LINE FITTING

Apart from the 23 C IV systems mentioned in Ellison et al. 1999b we have fitted another 5 C IV systems. We have detected one more system which is rather uncertain and we have not used it in this analysis. Fitted redshift values range from 2.376647 to 3.671271. The latter value corresponds to a radial velocity of $\sim -1.5 \times 10^4 \text{ km s}^{-1}$ with respect to the QSO. This reasonably ensures that the corresponding absorbers are intervening.

The lines were fitted by means of the Voigt profile fitting programme VPFIT (Webb 1987; Cooke 1994;

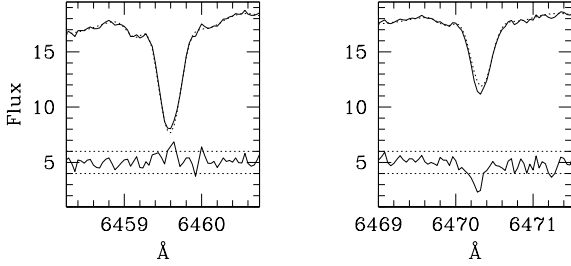


Figure 1. Example of C IV doublet showing an ADR. The *left* panel is for the 1548 Å line and the *right* panel for the 1550 Å line. In each panel from top to bottom shown are data (*solid* line) and fit (*dotted* line), and residuals (*solid* line) with $\pm 1\sigma$ level marked by two horizontal, *dotted* lines. Flux units are arbitrary.

<http://www.ast.cam.ac.uk/~rfc/vpfit.html>) which uses χ^2 minimization to produce lists of $b = \sqrt{2}\sigma$ (where σ is the standard deviation in a Gaussian distribution of velocities for the absorbing atoms), column density, $\log N$, and redshift, z , for all lines fitted. Where the C IV lines of interest were blended with transitions at different redshifts all lines were fitted together to produce a self-consistent fit. The wavelengths and oscillator strengths used for the C IV doublet are from Griesmann & Kling (2000). In some cases the lines of interest were blended with atmospheric transitions which were identified by means of the standard stars and an atmospheric line database. In order to obtain a satisfactory fit in the region of interest, we fitted the atmospheric transitions with Voigt profiles labelled ‘??’, which were assigned the Lyman α rest wavelength and oscillator strength. This option was also used in a few cases where it has not been possible to identify absorption features with certainty. In all, we have fitted 100 C IV doublets in the 28 systems which fall within the redshift interval mentioned above.

4 MODEL

4.1 Motivation

For a number of C IV doublets the fit showed a tendency to be below the data points for the 1548 Å line and above the data points for the 1550 Å line. This was an indication that the optical depth 2:1 ratio of the model profile was not adequate for the particular doublet, and it was a manifestation of an ADR, as mentioned above (see Figure 1). The fitting parameters for such lines are shown in Table 1. We stress that, short of including many extremely narrow and unphysical lines ($b \ll$ instrumental resolution), the only way to compensate for the effect is to adjust the zero level. In particular, the effect cannot be attributed to continuum uncertainties in the region of these lines. The zero level for a *given* line which shows an ADR is effectively ‘stretched’ by the addition of a term, whose value is determined iteratively during the fitting process. This does not affect the zero level of any other lines which do not show an ADR, regardless of how close in velocity space these may be to the adjusted line. This adjustment can thus selectively compensate for excess flux due to partial coverage from some, but not all, absorbing clouds.

4.2 Theoretical Considerations

We now show how an ADR follows from relatively straightforward partial coverage theory.

For a given true optical depth, $\tau_{\text{true}} \propto \frac{N}{b}$, when there is partial coverage, the observed intensity at a given wavelength is given by

$$I = (1 - f)I_0 + fI_0e^{-\tau_{\text{true}}} \equiv I_0e^{-\tau_{\text{obs}}} \quad (1)$$

where $f \equiv \frac{\text{Flux}_{\text{covered}}}{\text{Flux}_{\text{total}}}$ is the covering factor, I_0 is the unabsorbed continuum intensity and τ_{obs} is the optical depth that corresponds to the observed line profile. In what follows we shall use the label F to indicate a covering factor value obtained by means of *observed* and *known* image fluxes.

It then follows that for a doublet

$$I_1 = e^{-\tau_1} = 1 - f + fe^{-\tau_{\text{strong}}} \quad (2)$$

$$I_2 = e^{-\tau_2} = 1 - f + fe^{-\tau_{\text{weak}}} \quad (3)$$

where τ_{strong} (τ_{weak}) is the true optical depth of the strong (weak) component, τ_1 , τ_2 are the observed (apparent) optical depths and I_1 , I_2 are the observed residual intensities (normalized by the local continuum, I_0) at the same velocity for the strong and weak component of the doublet, respectively.

If the lines are optically thin, then from these exact expressions the relation

$$f = \frac{1 + I_2^2 - 2I_2}{1 + I_1 - 2I_2} \quad (4)$$

can be obtained which relates the covering factor to the observed residual intensities (Hamann & Ferland 1999). In what follows we shall use the label R to indicate a covering factor value obtained by means of *measured continuum normalized residual intensities*. All lines for which an adjustment of the zero level has been performed with VPFIT are listed in Table 1. The zero level adjustment, determined with VPFIT, as a fraction of the continuum is given in column 7 and its 1σ error in column 8. The covering factor determined from Equation 4, f_R , for these lines is given in column 9 of the Table. In principle, since the zero level adjustment is introduced to compensate for an excess continuum flux, the value for this adjustment should be in agreement with $1 - f_R$. The last column in Table 1 shows the value of $1 - f_R$ for all entries, f_R , in column 9. In other words, the last column can be thought of as giving an ‘expected’ adjustment based on the residual intensities. If one then compares corresponding entries in columns 7 (actual adjustment used) and 10 (expected adjustment from residual intensities), one may notice that these agree to within 1σ for line 17, to within $\gtrsim 1\sigma$ for lines 1, 4 and 15, and to within 2σ or more for the rest of the lines. We call this an R-type comparison (see below) and we shall return to this point later.

Further, from Equations 2 and 3 it is clear that the ratio of the observed optical depths, τ_1/τ_2 , depends both on f and on the true optical depth for each component, and thus, for given b , on the column density. This *theoretical* result is illustrated in Figure 2 for a line with $b = 10 \text{ km s}^{-1}$ and different values of the column density and covering factor. It can be seen that for low column densities and/or high covering factors, this ratio is close to 2. This corresponds to the case where an ADR is not observable. However, for given f and b there is a threshold in column density, above which

Table 1. Lines for which there is need for a zero level adjustment. Columns 7 and 8 indicate the adjustment, as a fraction of the continuum, and the corresponding error, respectively. Column 9 gives the covering factor calculated from the continuum normalized residual intensities via Equation 4. The entries in Column 10 have been calculated directly from corresponding entries in Column 9. The index numbers refer to the full table of intervening C IV lines fitted as explained in the text. Lines whose index numbers are prefixed by an x have not been used in this analysis because the zero level adjustment does not correspond to the covering factor of ~ 0.4 assumed in our model.

Index	z	b	σ_b	$\log N$	$\sigma_{\log N}$	Adjustment	Error	f_R	$1 - f_R$
1	3.108227	4.6	7.3	12.66	1.77	0.54	0.11	0.589547	0.410453
2	3.108299	12.8	18.0	13.07	1.31	0.54	0.11	0.652179	0.347821
3	3.108377	5.1	1.7	13.40	0.37	0.54	0.11	0.788434	0.211566
4	3.109511	10.8	1.4	13.45	0.06	0.54	0.11	0.580464	0.419536
13	3.134610	12.9	3.7	12.68	0.17	0.69	0.04	0.069223	0.930777
14	3.135135	16.1	2.0	12.96	0.07	0.69	0.04	0.082394	0.917606
15	3.133197	32.4	15.7	13.48	0.21	0.69	0.04	0.097442	0.902558
16	3.132676	13.3	4.4	12.94	0.31	0.69	0.04	0.097617	0.902383
17	3.133632	9.6	1.4	13.65	0.10	0.69	0.04	0.328090	0.671910
x15	3.172332	6.6	0.2	13.42	0.03	0.28	0.03	0.773285	0.226715
x28	3.202986	32.0	2.0	13.63	0.06	0.50	0.04	0.611514	0.388486
x29	3.202999	6.9	0.8	13.10	0.10	0.50	0.04	0.646416	0.353584

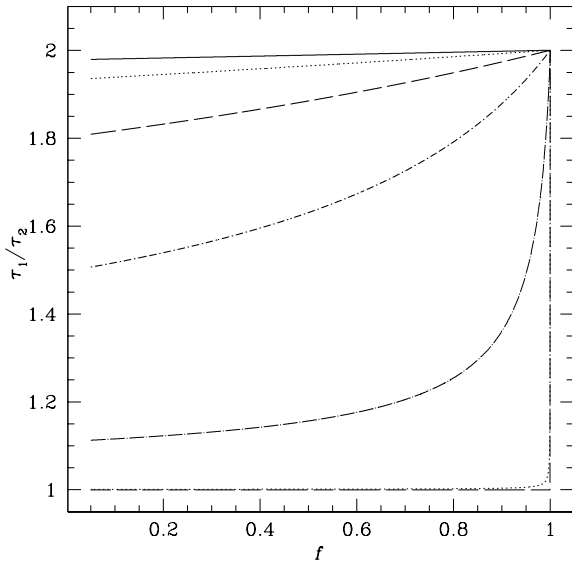


Figure 2. Theoretical ADR. Shown here is the ratio of observed optical depths, τ_1/τ_2 as a function of covering factor f and $\log N(\text{C IV})$ for a C IV line with $b = 10 \text{ km s}^{-1}$. From top to bottom, the curves are for $\log N(\text{C IV})$ of 12.0, 12.5, 13.0, 13.5, 14.0, 14.5, 15.0.

the ratio will deviate significantly from 2 and, depending on the SNR in the region of the line, it will not be possible to fit the line with a model Voigt profile (which assumes a ratio of 2) without obtaining large residuals. This effect is seen in Figure 1: relative to τ_2 , τ_1 is less than what VPFIT expects and, hence, the fit appears markedly below the 1548 Å line and above the 1550 Å line.

4.3 Simulating an ADR

This discrepancy is due to excess flux getting through at the velocity where a particular doublet is observed. If the true optical depth and the covering factor are known, the observed, continuum normalized intensity is given by Equations 2 or 3. Thus, although the *true* continuum normalized profile is $e^{-\tau}$, the profile actually *observed* will be

$$\frac{1-f}{f} + e^{-\tau}. \quad (5)$$

This Equation is really the same as Equation 2 (or Equation 3) but with a different normalization. In practice this means that, if one wishes to simulate this effect for various values of the true optical depth and covering factor, one needs to add a constant $\alpha \equiv \frac{1-f}{f}$ to a continuum normalized spectrum. For example, if there are two LOS of equal brightness and one is fully covered while the other is uncovered, then $f = 0.5$, $\alpha = 1$ and if one starts with a given, true absorption profile in a unit continuum, the observable effects of partial coverage, if any, will be reproduced if one adds a constant = 1 to all data points. The different normalization of Equation 5 is convenient because excess flux can be expressed in terms of a single additive constant, α .

Thus a choice needs to be made on an appropriate value for f (or, equivalently, α) since this is necessary for simulating an ADR. In particular, in the case of APM 0827+5255 the most plausible lensing model (Egami et al. 2000, Ibata et al. 1999), as well as recent observations with the Hubble Space Telescope (Lewis et al. 2002), indicate that the lensed system is made up of three images, A, B and C, for which the flux ratio is $A : B : C = 1 : 0.773 : 0.175$. However, image C lies closer to A, so A is less likely to be the only one covered. Therefore, it is plausible to assume that in most cases there are, effectively, two images, A+C and B, either of which, or both, may be covered by intervening absorbers. Also, since C contributes less than 10% of the total flux, its presence (or absence) will make little difference to the

ADR. There is also further, more quantitative evidence that such a partial coverage configuration is plausible. This was obtained as follows:

In Table 2 we have tabulated all partial coverage combinations which, from a geometric point of view, are reasonably probable. From the known multiple image fluxes we calculated the covering factors, f_F , and the corresponding ‘expected zero level adjustments’, $1 - f_F$, for each partial coverage configuration. We then compared the latter with columns 7 and 8 (*actual* adjustment performed, \pm error) of Table 1 (we call this a comparison of ‘type F’). This comparison suggests that, among the simple partial coverage models in Table 2, the one with $\alpha = 1.520$ ($f \sim 0.4$) provides the best physical basis for most of the adjustments presented in Table 1, except those whose index number is marked by an x. Alternatively, it is possible to compare the last column of Table 1 (‘expected zero level adjustment’, $1 - f_R$, *from the residual intensities*) to columns 7 and 8 of the same Table (we call this a comparison of ‘type R’). However, for any given line, f_R is likely to be less reliable than f_F as it depends on the residual intensity measured, which is strongly affected by blending due to other nearby lines. We have thus not based our choice of model on an R-type comparison. Nevertheless, it is interesting to note that for line x15 which is only moderately blended, no simple model among those shown in Table 2 comes close to being acceptable, on the basis of an F-comparison. However, this line is only moderately blended, and an R-comparison shows that corresponding values in columns 7 and 10 of Table 1 *are* fairly close. There is thus little doubt about the reality of the effect, but, perhaps, there is a more complicated physical situation which requires more sophisticated modelling. On the other hand, model ‘A covered, B+C uncovered’ would be adequate for lines x28 and x29 (on the basis of our chosen F-comparison). In any case, we chose not to discard lines for which there was poor agreement between columns 7 and 10 of Table 1 (the R-comparison failed) as they might provide useful insight after the simulations were complete.

To summarise, by performing Voigt profile fitting of intervening C IV lines, we have obtained a sample of 100 fitted b -log N pairs. For 12 of these lines an ADR was present and an adjustment of the zero level has been applied in order that a good fit be obtained. We have chosen a set of 4 possible partial coverage configurations for this object and, using the known flux ratios of the three images, have obtained 4 values for $1 - f_F$, the ‘expected zero level adjustment’. One of these values agrees best with the greatest number of adjustments actually imposed on the 12 fitted lines. We thus chose the corresponding model ($f \sim 0.4$) as the best candidate for a physical explanation of the observed ADR.

5 SIMULATIONS

5.1 Need for Simulations

A reliable way of establishing that the chosen partial coverage model can (or cannot) give rise to a detectable ADR for a given b -log N -SNR combination is to perform a set of simulations, as explained in the next subsection.

Once the detectability, or not, of the ADR has been established, this can be compared to the *actual* situation in

the observed spectrum. For each b -log N -SNR combination there are four possibilities:

- (i) ADR *not* detectable and *not* seen in observed spectrum,
- (ii) ADR detectable *and* seen in observed spectrum,
- (iii) ADR detectable but *not* seen in observed spectrum,
- (iv) ADR *not* detectable *but* seen in observed spectrum.

Cases (ii) and (iii) are useful for estimating absorber sizes: In case (ii) *partial* coverage is established and, therefore, the transverse size of the absorber must be *smaller* than the proper separation of the LOS at the absorbing redshift. Conversely, in case (iii) *total* coverage is established and the transverse size of the absorber must be *larger* than the proper separation of the LOS.

Further, a maximum likelihood approach can be used to estimate most probable absorber sizes from the number of established partial and total coverage cases.

5.2 Method

Each of the 100 fitted b -log N pairs mentioned above gives a single *true* τ value and can be used to produce an artificial continuum normalized absorption profile, $e^{-\tau}$. If one adds a term $\alpha = 1.520$ to each data point in this profile, one effectively introduces excess flux due to partial coverage from our chosen physical model (Equation 5).

Because the SNR varies considerably over the observed spectrum from ~ 25 to ~ 120 , for each region containing a C IV doublet component an average SNR value was determined by inspection of the spectrum using the task *splot* in IRAF.

For each b -log N (C IV) pair two artificial spectra were produced. The first spectrum contained 120 C IV doublets with a profile $e^{-\tau}$. The spacing of the lines was chosen empirically so that when subsequently the lines would be fitted with VPFIT, blending complications would be absent, i.e. even the broadest lines were well apart from each other. The spectrum was resampled to the resolution of the observed spectrum (0.04 Å per pixel) and smoothed to the instrumental resolution of 6.6 km s⁻¹. Gaussian noise was added with $\sigma = \frac{1}{\text{SNR}}$ to obtain the desirable final SNR, as measured beforehand for each region.

The above process was repeated to produce another set of 120 simulations of the same line aiming to reproduce the effects of excess flux. This time gaussian noise with $\sigma = \frac{1+\alpha}{\text{SNR}}$ was added to the unit continuum spectrum and both data and continuum were then increased by α . This ensured that the desired SNR was obtained in this case as well.

Next, VPFIT was used to fit the artificial spectra. Each of the 120 artificial doublets in the spectrum was fitted independently, so that 120 separate χ^2 values were obtained. The starting b -log N values for the VPFIT iterations were exactly the same as those used to make the simulated lines, so that one would expect to obtain a good fit, unless the effects of excess flux were significant.

VPFIT was allowed to fit only a single Voigt profile to each simulated line. The option of automatically putting in additional narrow lines to improve poor fits was not used since such lines were known to be spurious by construction. The fitting region for each doublet component was centred on the component ‘redshift’ and extended over $3 \times \text{FWHM}$,

Table 2. Possible partial coverage models for APM 0827+5255. From *left to right* columns give the covering factor, f_F , calculated from the flux ratio A : B : C = 1 : 0.773 : 0.175, the value of $1 - f_F$ which, ideally, should be in good agreement with the adjustment of the zero level that needs to be performed to obtain a good Voigt profile fit if an ADR is observed, the image assumed covered, the image not covered and the constant, $\alpha \equiv \frac{1-f}{f}$, that has to be added to a continuum normalized absorption spectrum to simulate excess flux.

f_F	$1 - f_F$	image covered	image not covered	α
0.397	0.603	B	A+C	1.520
0.487	0.513	B+C	A	1.055
0.513	0.487	A	B+C	0.948
0.603	0.397	A+C	B	0.659

Table 3. Lines for which simulations indicated that an ADR is detectable. Columns 2 to 6 give the fitting parameters for the observed lines. Column 7 gives the significance for the KS statistic. The last column indicates whether the result means there is partial (*p*) or total (*t*) coverage.

Index	z	b	σ_b	$\log N$	$\sigma_{\log N}$	Significance	Coverage
3	3.108377	5.1	1.7	13.40	0.37	< 0.001	<i>p</i>
4	3.109511	10.8	1.4	13.45	0.06	< 0.001	<i>p</i>
7	3.108564	18.6	1.6	13.53	0.08	< 0.001	<i>t</i>
15	3.133197	32.4	15.7	13.48	0.21	< 0.04	<i>p</i>
17	3.133632	9.6	1.4	13.65	0.10	< 0.001	<i>p</i>
18	3.134133	12.6	0.8	13.14	0.05	< 0.05	<i>t</i>
25	3.172054	6.3	1.1	12.25	0.06	< 0.05	<i>t</i>
26	3.172580	17.5	3.2	12.57	0.08	< 0.04	<i>t</i>
45	3.377585	9.8	0.3	13.20	0.02	< 0.001	<i>t</i>
96	2.974079	9.1	0.4	13.19	0.02	< 0.03	<i>t</i>

where $\text{FWHM} = 2\sqrt{\ln 2} b$ is the full width at half minimum. This was done to avoid including too much continuum which can make a poor fit less pronounced.

If for a given b - $\log N$ pair the higher continuum introduced an observable ADR, then, on average, the second set of 120 fits should be markedly poorer than the first set. Otherwise, the two distributions of χ^2 (reduced) obtained should not differ significantly. Figure 4 shows a single simulation of line 3 with the Voigt profile fit superposed. An ADR was reproduced at $> 2\sigma$ level in the central region of the line. Note that a 2 : 1 doublet ratio was recovered for this simulated line when the zero level was adjusted by 0.62 ± 0.02 , which agrees both with the original adjustment of 0.54 ± 0.11 (Table 1) and with $1 - f_F = 0.603$ for a simulated line with $\alpha = 1.520$ (Table 2). Independently from this result from VPFIT, the continuum normalized residual intensities gave a covering factor $f_R = 0.378$ ($1 - f_R = 0.622$), also in good agreement. Additionally, the original Voigt parameters of the line were recovered after the adjustment of the zero level ($b = 5.0 \pm 0.2 \text{ km s}^{-1}$, $\log N = 13.44 \pm 0.05$; compare with Table 1). This shows that this type of adjustment successfully compensates for partial coverage effects and that using fitted b - $\log N$ values to simulate lines with an adjusted zero level is physically meaningful.

For each simulated b - $\log N$ pair we performed a two-sided Kolmogorov–Smirnov (KS) test for the two cumulative distributions, C_1 and $C_{1+\alpha}$ of χ^2 (reduced) obtained, in order

to see if the ADR had been reproduced, in a statistically significant sense, by the simulations. If the significance level for the KS statistic, defined as $D \equiv \max |C_1(\chi^2) - C_{1+\alpha}(\chi^2)|$, was less than 0.05, the null hypothesis that the two distributions were the same was discarded. This was interpreted as evidence that the second set of 120 fits was poorer and thus an ADR had been reproduced. The significance results for all such lines are given in Table 3. We illustrate by plotting the cumulative distributions of the χ^2 values for fits to simulations of line 3 in Figure 3.

If the corresponding originally fitted line also showed an ADR [case (ii) in Section 5.1], the assumed partial covering model was taken to be the physical reason (a *p*-case. In work where separate spectra are available for each LOS the term ‘anticoincidence’ is commonly used for such cases). On the other hand, if the effect appeared *only* in a simulation [case (iii) in Section 5.1], then, as far as this model was concerned, there was no partial but total coverage (a *t*-case or ‘coincidence’ in work with separate spectra).

In Section 6 we explain how we used the number of *t* and *p*-cases to obtain an estimate for the absorber sizes for two distinct absorber geometries.

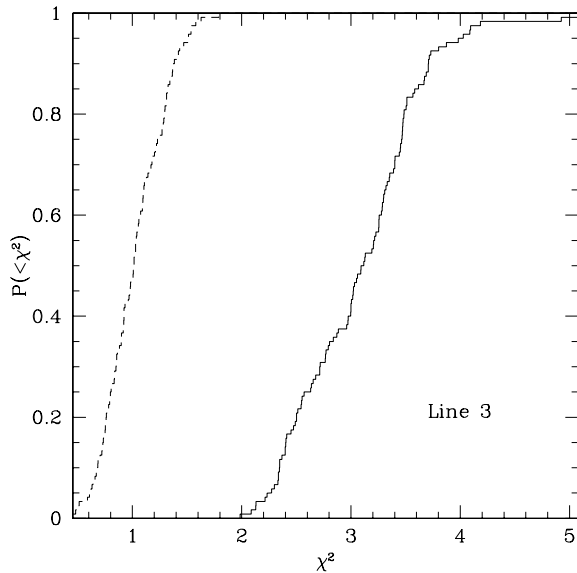


Figure 3. Cumulative distribution of reduced χ^2 for Voigt profile fits to simulated line 3. *Solid* line: distribution of 120 χ^2 values from fits to simulated doublets with a continuum $1 + \alpha$. *Dashed* line: distribution of 120 χ^2 values from fits to simulated doublets with a unit continuum.

5.3 Results

According to the reasoning above, for $\alpha = 1.520$ Table 3 establishes the detectability of the ADR for the 10 simulated lines listed there, of which 6 did not show the effect in the observed spectrum (and were thus taken to be *t*-cases) and 4 also showed the effect in the observed spectrum (*p*-cases).

More generally, all fitted and simulated lines can be divided into the four groups introduced in Section 5.1:

(i) For the majority of lines no ADR was detected either during Voigt profile fitting or in simulations. Such lines were not used further (but see discussion).

(ii) For lines 3, 4, 15 and 17 the zero level has been adjusted during fitting and the ADR was reproduced in simulations. These *p* lines are indicated by *solid* ticks in Figures 5 and 6. These lines belong to each of the two systems ($z \approx 3.10$ and $z \approx 3.13$) that show the effect *and* were used in this analysis (see Table 1).

(iii) For lines 7, 18, 25, 26, 45 and 96 an ADR was only produced in simulations with varying degrees of significance. Lines 7 and 18 are from the two systems at $z \approx 3.10$ and $z \approx 3.13$ for other lines of which partial coverage was suggested by the simulations. Lines 25 and 26 belong to the $z \approx 3.17$ system in which line x15 shows an ADR which cannot be modelled with $\alpha = 1.520$. Lines 45 and 96 are from lower redshift systems. These *t* lines are indicated by *dot-short-dashed* ticks in Figures 5 to 9.

(iv) Finally, for lines 1, 2 ($z \approx 3.10$ system) and 13, 14, 16 ($z \approx 3.13$ system) an ADR was not reproduced in simulations although they have been fitted with a zero level adjustment. These lines are indicated by *long-dashed* ticks and numbers in Figures 5 and 6 and were not used further.

The existence of this last group of lines in a way pro-

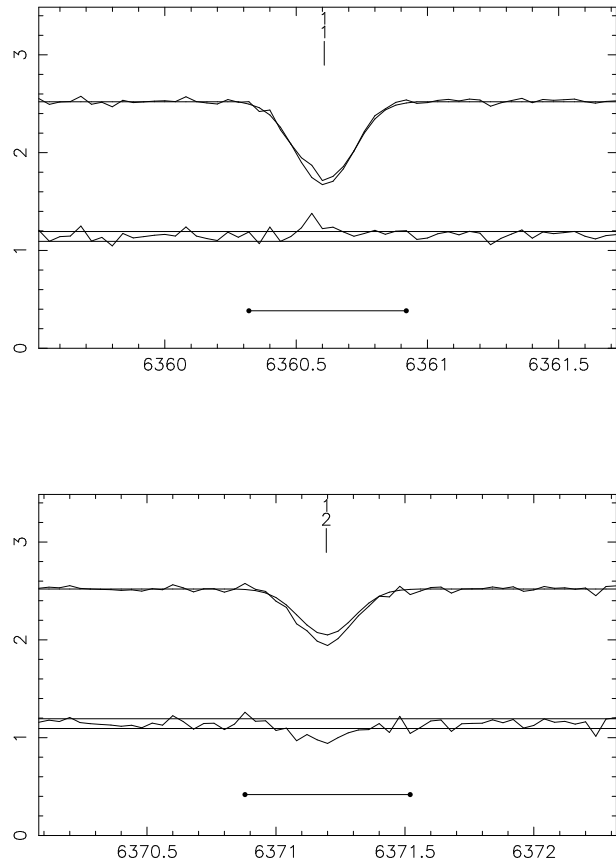


Figure 4. Simulated C IV doublet (*upper panel*: 1548 Å region, *lower panel*: 1550 Å region) showing an anomalous doublet ratio. The Voigt parameters for the line are the same as for line 3. Shown in each panel from top to bottom are data and fit, residuals with $\pm 1\sigma$ level marked by the two horizontal lines, and fitting region ($3 \times \text{FWHM}$). Note how, as in Figure 1, near the line centre, the fit appears below (above) the data in the 1548 Å (1550 Å) region.

vides an *a posteriori* justification of simulations. To check the effect that zero level adjustment of such lines had on the overall goodness-of-fit, we modified the fit for the $z \approx 3.10$ and 3.13 system as follows:

We used the last fitting results for each region as input to VPFIT but excluded group (iv) lines from zero level adjustment. Otherwise, we did not introduce any new lines. This procedure had a negligible effect on the fit for the $z \approx 3.10$ system (reduced χ^2 changed from ~ 1.09 to ~ 1.10). The original adjustment of the zero level for lines 1 and 2 was not necessary and was probably a result of the empirical nature of this adjustment combined with the fact that these lines are close to the stronger line 3. In the case of the $z \approx 3.13$ system and lines 13, 14 and 16 the situation is similar since the reduced χ^2 changed from ~ 1.16 to ~ 1.17 .

The simulations thus allowed us to distinguish for which lines an ADR may have a physical cause.

The choice of an upper limit for the significance of the KS statistic was somewhat arbitrary. We chose 5% in an effort not to discard too many lines, since few lines were available anyway. However, the χ^2 cumulative distribution plots for lines 25 and 26 strongly indicate that a lower value might be appropriate since χ^2 values for fits of simulated

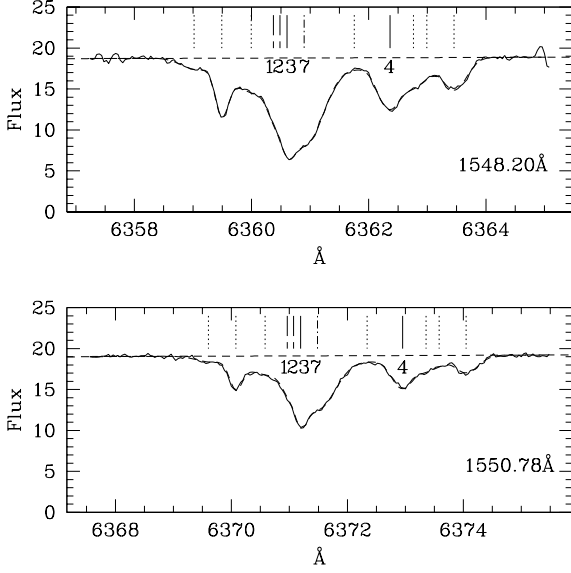


Figure 5. Fitted absorption lines which may be due to partial or total coverage of LOS to APM 0827+5255 as suggested by simulations for the $z \approx 3.10$ system. The fit is shown by a dashed line, superposed on the data. The horizontal dashed line shows the continuum. Numbers correspond to entries in Tables 1 and 3. *Solid* ticks and numbers indicate lines for which the zero level has been adjusted at the Voigt profile fitting stage (Table 1) and for which an ADR was reproduced in the simulations for this model. *Long-dashed* ticks and numbers indicate lines for which the zero level has been adjusted at the Voigt profile fitting stage but an ADR was not reproduced in the simulations. *Dot-short-dashed* ticks and numbers indicate lines for which the zero level has not been adjusted at the fitting stage but an ADR was reproduced in simulations when excess flux was introduced (Table 3). Other fitted C IV lines are indicated by *dotted* ticks.

lines with excess flux did not show a clear trend to be higher. Since we were mainly interested in illustrating a technique, we formally accepted the 5% level and used these two lines in further analysis. If this caveat is taken into account, Table 3 suggests that a threshold column density for an observable ADR in this model is given by $\log N(\text{C IV}) \gtrsim 13.1$ with $b \approx 10 \text{ km s}^{-1}$. This explains the failure to reproduce lines in group (iv) above since all of these lines (except, perhaps, for line 2, which, however, has large $\sigma_{\log N}$) are below this threshold.

6 ESTIMATING ABSORBER SIZES

6.1 Direct Estimates

Minimum size estimates can be obtained straightforwardly from lines which correspond to total coverage.

The proper separation at redshift z of the light paths from the two images of a lensed QSO with emission redshift z_{em} due to a lens at redshift z_1 is given by

$$S(z) = \frac{D(z_1, z_{\text{con}} = 0)D(z, z_{\text{em}})}{D(z_1, z_{\text{em}})} \delta\phi, \quad (6)$$

(Young et al. 1981) where $\delta\phi$ is the observed angular separation

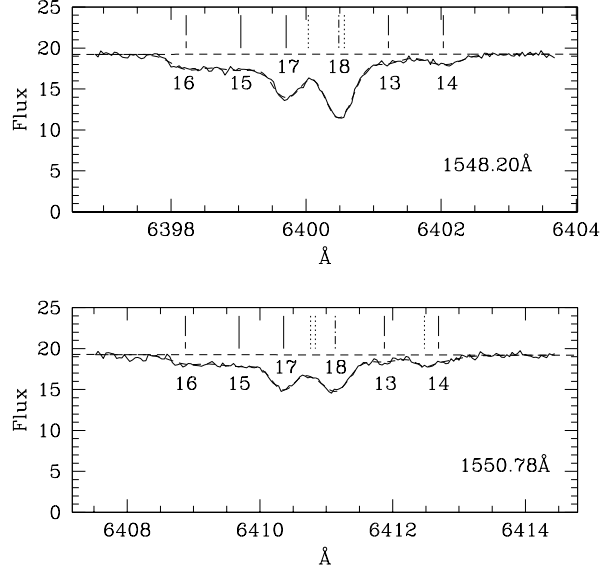


Figure 6. As in Figure 5 but for the $z \approx 3.13$ system. Only in this Figure *dotted* ticks indicate unidentified/atmospheric lines.

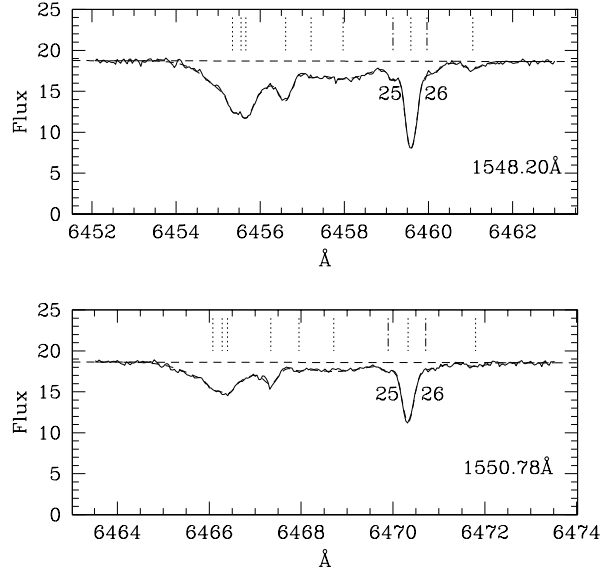


Figure 7. As in Figure 5 but for the $z \approx 3.17$ system.

of the images. The light paths converge at $z_{\text{con}} = 0$ and the angular diameter distances, D , are given by

$$D(z_1, z_2) = \frac{D_C(z_2) - D_C(z_1)}{1 + z_2} \quad (7)$$

where

$$D_C(z) = \frac{c}{H_0} \int_0^z \frac{dz'}{\sqrt{\Omega_M(1+z')^3 + \Omega_\Lambda}} \quad (8)$$

is the comoving distance for a flat universe ($\Omega_K = 0$; Peebles 1993; Hogg 2000). Equ. 6 holds for $z > z_1$ as assumed here.

Table 4. Minimum sizes for C IV absorbers. Columns 1 and 2 give the line index and fitted redshift for all coincidences established with simulations. Columns 3 to 7 give the separations of the two lines of sight for five different lensing redshifts. All separations are in h_{72}^{-1} kpc. Here $q_0 = 0.5$.

Index	z	$S(z_1 = 0.7)$	$S(z_1 = 1.062)$	$S(z_1 = 1.1727)$	$S(z_1 = 1.181)$	$S(z_1 = 2.974)$
7	3.108564	0.272	0.377	0.409	0.411	1.561
18	3.134133	0.262	0.363	0.394	0.396	1.504
25	3.172054	0.248	0.343	0.372	0.374	1.421
26	3.172580	0.248	0.343	0.372	0.374	1.420
45	3.377585	0.173	0.239	0.259	0.261	0.990
96	2.974079	0.326	0.451	0.489	0.492	1.868

Table 5. Same as Table 4 but for $\Omega_M = 0.3$, $\Omega_\Lambda = 0.7$.

Index	z	$S(z_1 = 0.7)$	$S(z_1 = 1.062)$	$S(z_1 = 1.1727)$	$S(z_1 = 1.181)$	$S(z_1 = 2.974)$
7	3.108564	0.362	0.518	0.566	0.570	2.317
18	3.134133	0.349	0.499	0.546	0.549	2.233
25	3.172054	0.330	0.471	0.516	0.519	2.110
26	3.172580	0.329	0.471	0.515	0.519	2.108
45	3.377585	0.230	0.329	0.359	0.362	1.471
96	2.974079	0.433	0.619	0.677	0.681	2.770

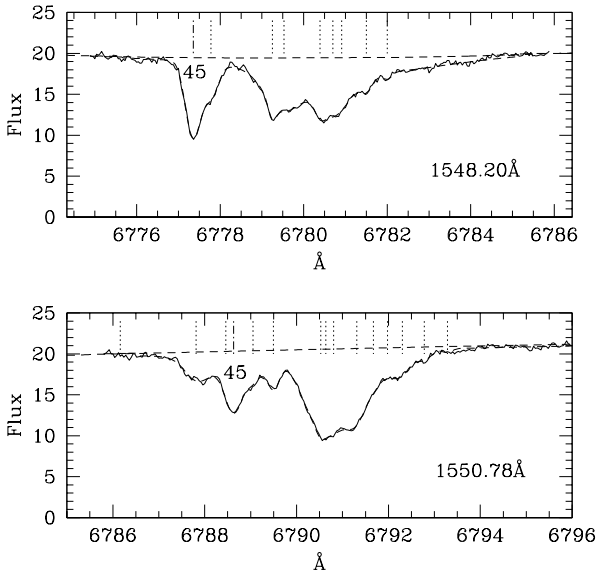


Figure 8. As in Figure 5 but for the $z \approx 3.37$ system.

Egami et al. (2000) argue that the lensing galaxy should be at $z_1 \sim 3$ based on the Einstein and core radii of their model. The damped Lyman α system at $z \sim 2.974$ may be compatible with this estimate. Additionally, Petitjean et al. (2000) suggest that strong Mg II systems are prime lense candidates because the roughly equal brightnesses of images A and B suggest the LOS are traversing the central regions of the lensing object. We have thus calculated the

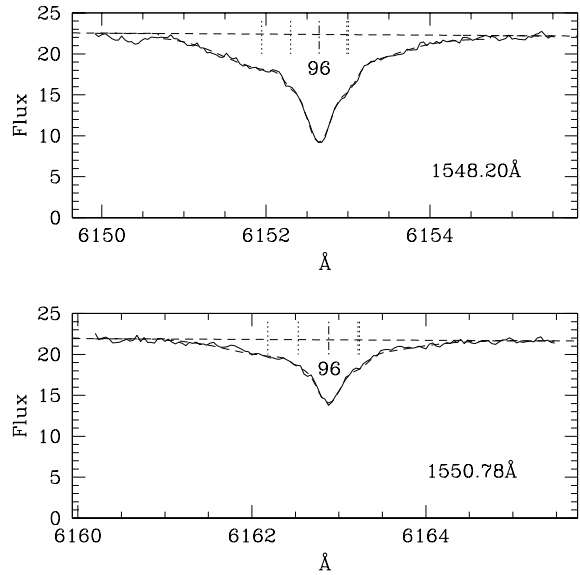


Figure 9. As in Figure 5 but for the $z \approx 2.97$ system.

separation for five values of z_1 as shown in Tables 4 and 5. These values include an arbitrary value of 0.7, not corresponding to any known object, three values corresponding to observed Mg II systems and one value from the damped Lyman α system mentioned. The observed angular separation of image B from the combined A+C image was taken to be $\delta\phi = 0.369$ arcsec. There is some ambiguity as to what one means by the location of the A+C image, and we have simply chosen the location of the flux-weighted cen-

troid of the A+C image. Size estimates scale with $\delta\phi$ (this still holds, approximately, in the statistical approach of the next section) and so the effect is of the order of no more than a few percent. Thus the results remain qualitatively unaffected.

6.2 Maximum Likelihood Analysis

We then applied a maximum likelihood method in order to estimate the most probable size of the absorbers, given the information that we have obtained through this work. We assumed two simple geometries for absorbers of uniform size.

The probability that a *spherical* cloud is intersected by both LOS, given that it is intersected by one is

$$\phi_s(X) = \frac{2}{\pi} \left\{ \arccos [X(z)] - X(z) \sqrt{1 - X(z)^2} \right\} \quad (9)$$

(McGill 1990), for $X \in [0, 1]$, and zero otherwise. Here $X(z) \equiv S(z)/2R$, where R is the absorber radius. For randomly inclined circular disks the probability is

$$\phi_d(X) = \int_{-\pi/2}^{\pi/2} \frac{\cos \theta}{\pi} \times \left\{ \arccos \left[\frac{X(z)}{\cos \theta} \right] - \frac{X(z)}{\cos \theta} \sqrt{1 - \frac{X(z)^2}{\cos^2 \theta}} \right\} d\theta \quad (10)$$

for $X < \cos \theta$ and zero otherwise (McGill 1990). Here θ is the angle of inclination of the disk relative to the lines of sight. We were actually interested in the case where there is absorption at *either* LOS, so that the probability that there is absorption at the other LOS is

$$\psi_{s,d} = \frac{\phi_{s,d}}{2 - \phi_{s,d}} \quad (11)$$

[by analogy to Dinshaw et al. (1997) who apply this to two separate spectra]. The probability of getting the estimated number of cases where there is coverage of one or both lines of sight is then given by the likelihood function

$$\mathcal{L}(R) = \prod_i \psi_{s,d} [X(z_i)] \prod_j \{1 - \psi_{s,d} [X(z_j)]\}, \quad (12)$$

where i labels cases of total coverage (t lines) and j cases of single coverage (p lines).

The results of the likelihood analysis for different lensing redshifts are summarized in Figure 10 and Tables 6 and 7. The plots show the differential likelihood distributions for the two assumed geometries, $\mathcal{L}(R)$, which peak at the most probable radii for given z_1 . Also plotted are the cumulative distributions from which median R values have been calculated together with 95% confidence intervals. For spherical absorbers in a non-zero Λ universe the most likely sizes ($2R$) are in the range from 1.74 to 9.26 h_{72}^{-1} kpc. Median sizes are in the range from 2.6 to 13.9 h_{72}^{-1} kpc. For randomly inclined disks the most likely sizes lie between 2.56 and 13.58 h_{72}^{-1} kpc. Median sizes are between 3.92 and 20.84 h_{72}^{-1} kpc. In a zero Λ universe these values are smaller by a factor of ~ 1.4 .

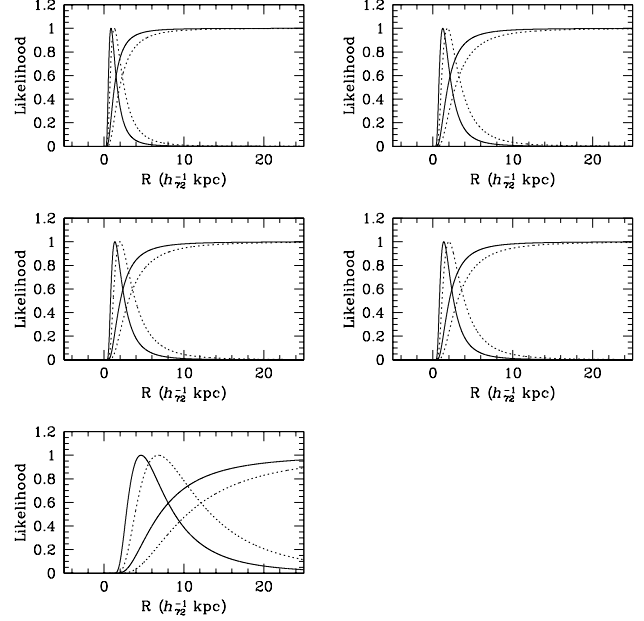


Figure 10. Differential and cumulative likelihood distributions for spherical absorbers (*solid curves*) and randomly inclined disks (*dotted curves*) as functions of cloud radius in an $\Omega_M = 0.3$, $\Omega_\Lambda = 0.7$ universe. The differential distribution has been normalized to its peak value. From left to right and top to bottom results are shown for z_1 of 0.7, 1.062, 1.1727, 1.181, 2.974.

7 DISCUSSION

We have used a simple model to select candidate lines for which the ADR is due to coverage of one LOS. Our model only considered two LOS, the corresponding images to which, nevertheless, are not equally bright. As in previous work on the subject, only two simple geometries have been considered for the absorbing structures. These geometric assumptions are simple not only in terms of the assumed shapes but also in that these structures more realistically should have no sharp edge: even in the simplest scenario the column density has a profile which falls smoothly radially outwards. Thus the absorbers giving rise to lines x15, x28 and x29 may conceivably have the same column density profile as the rest but they may be positioned with respect to a LOS in such a way that they present a different covering factor. However, incorporation of such more realistic models is only possible when separate spectra for different LOS are available (e.g. D'Odorico et al. 1998, Rauch et al. 2001).

The use of simulated spectra to reproduce an ADR is crucial because the observed ADR by itself does not provide enough information to establish the partial coverage effect. For example, group (iv) lines did not show an ADR when simulated. Also the magnitude of the adjustment does not necessarily constrain the model sufficiently. As explained, in theory one would expect the adjustment to agree with $1 - f_R$ calculated from the residual intensities (columns 7 and 10 in Table 1). In practice, this was not always the case. This was probably due to blending with nearby lines. Blending affects the observed residual intensities at the velocity position of the line of interest, leading to an inaccurate value for $1 - f_R$. It may also have an effect on the magnitude of the adjust-

Table 6. Radius estimates of CIV absorbers from maximum likelihood analysis in an $\Omega_M = 1$, $\Omega_\Lambda = 0$ universe. The most probable and median radii for spherical clouds and randomly inclined disks are shown for four different lensing redshifts. The 95% confidence limits have been estimated from the cumulative distributions.

z_1	Spheres			Disks		
	Mode R (h_{72}^{-1} kpc)	Median R (h_{72}^{-1} kpc)	95%	Mode R (h_{72}^{-1} kpc)	Median R (h_{72}^{-1} kpc)	95%
			Confidence Limits (h_{72}^{-1} kpc)			Confidence Limits (h_{72}^{-1} kpc)
0.7000	0.650	0.980	0.380-4.330	0.960	1.480	0.540-6.900
1.0620	0.900	1.360	0.540-6.210	1.330	2.040	0.740-9.140
1.1727	0.980	1.470	0.570-6.470	1.440	2.210	0.790-9.850
1.1810	0.980	1.480	0.580-6.570	1.450	2.230	0.810-10.230
2.9740	3.120	4.680	1.810-20.150	4.570	7.030	2.510-31.000

Table 7. Same as Table 6 but for an $\Omega_M = 0.3$, $\Omega_\Lambda = 0.7$ universe.

z_1	Spheres			Disks		
	Mode R (h_{72}^{-1} kpc)	Median R (h_{72}^{-1} kpc)	95%	Mode R (h_{72}^{-1} kpc)	Median R (h_{72}^{-1} kpc)	95%
			Confidence Limits (h_{72}^{-1} kpc)			Confidence Limits (h_{72}^{-1} kpc)
0.7000	0.870	1.300	0.500-5.610	1.280	1.960	0.710-8.760
1.0620	1.240	1.860	0.720-8.090	1.830	2.800	1.010-12.470
1.1727	1.360	2.040	0.800-9.140	2.000	3.070	1.110-14.000
1.1810	1.360	2.050	0.800-9.030	2.010	3.090	1.120-14.090
2.9740	4.630	6.950	2.690-29.890	6.790	10.420	3.720-44.670

ment performed, leading to further discrepancy between the values in columns 7 and 10. For example, line 3 (adjustment = 0.54 ± 11 , $1 - f_R = 0.211566$) was simulated with an ADR but lies 5.7 km s^{-1} from line 2 ($b = 12.8 \text{ km s}^{-1}$, $\log N = 13.07$) and 13.6 km s^{-1} from line 7 ($b = 18.6 \text{ km s}^{-1}$, $\log N = 13.53$). Although when simulated and fitted the line was in excellent agreement with the $\alpha = 1.520$ model, for the observed and fitted line there was some discrepancy (though not within the error) between actual adjustment and $1 - f_F$, and a more serious discrepancy between actual adjustment and $1 - f_R$. Of course some degree of agreement is necessary, at least between $1 - f_F$ and actual adjustment. As explained before, this is how we chose the best value of α for our simulations.

On the other hand, line 17 does not suffer from as much blending, is stronger and the discrepancy is smaller.

More insight on the threshold Voigt parameters a line needs to have for partial coverage to lead to an observable ADR, and on the reality of the effect can be obtained by inspection of group (i) lines. Specifically, such lines should be below the estimated threshold mentioned above (Section 5.3), in that one or more of the following are true: The lines have low $\log N$, large b , or they lie in a region with low SNR. Parameters for all group (i) lines with $\log N(\text{CIV}) \geq 13.0$ are shown in Table 8. It can be seen that usually lines are too broad for their column density. For line 93 the problem may be aggravated by a relatively low SNR.

Given the small size of the sample, these results cannot

be considered representative of intervening CIV absorbers in general. Rather they should be considered as an illustration of what can be learned from a compilation of similar studies of gravitationally lensed QSOs. From Equations 9 to 12 it follows that these results depend on LOS separations for the sample lines and on lensing redshifts chosen. However, taken at face value they strongly suggest that *CIV absorption arises in structures with sizes on the order of kiloparsecs*. It can be seen from Tables 6 and 7 that, for the three z_1 values 1.062, 1.1727 and 1.181, estimated sizes are of the order of ~ 2 kpc. On the other hand, Tables 4 and 5 suggest that the structures responsible for intervening CIV absorption cannot be smaller than $\sim 0.2h_{72}^{-1}$ kpc for $\Omega_M = 1$, $\Omega_\Lambda = 0$ ($\sim 0.3h_{72}^{-1}$ kpc for $\Omega_M = 0.3$, $\Omega_\Lambda = 0.7$).

Up to this point we have implicitly assumed that the estimated ‘sizes’ are those of coherent, discrete entities. In particular, the maximum likelihood method is based on an assumption about the geometric shape of such objects. However, whether one has separate spectra for different LOS or not, the same observations can also be due to an ensemble of correlated objects of smaller characteristic size. In this case total coverage provides an estimate for a coherence length of clustered absorbers. Alternatively, there might be a lack of discrete objects at any scale, with partial coverage being the effect of variations in an inhomogeneous density field permeating the IGM.

If total coverage is due to correlated discrete absorbers, then in practice we may be ‘measuring’ transverse sizes of

Table 8. Lines with $\log N(\text{C IV}) \geq 13.0$ for which an ADR was neither observed in the fitted spectrum nor generated in the simulations. Symbols have the same meaning as in previous tables. The last two columns give the average SNR in the 1548 and 1550 Å regions.

index	z	σ_z	b	σ_b	$\log N$	$\sigma_{\log N}$	SNR ₁₅₄₈	SNR ₁₅₅₀
12	3.107982	0.000034	24.8	10.6	13.137	0.146	95	95
21	3.169724	0.000011	41.3	1.4	13.439	0.010	75	100
24	3.171289	0.000032	44.1	4.6	13.089	0.039	75	100
41	3.384759	0.000041	38.0	2.7	13.018	0.038	85	85
43	3.386163	0.000011	26.9	0.9	13.534	0.015	85	85
47	3.378988	0.000026	26.1	1.8	13.273	0.028	85	85
48	3.379746	0.000029	22.9	2.3	13.251	0.055	85	85
59	3.502039	0.000000	12.6	0.4	13.010	0.014	90	90
67	3.558324	0.000037	16.1	1.7	13.323	0.121	80	80
68	3.558079	0.000006	6.5	1.1	13.107	0.170	80	80
78	3.655437	0.000074	163.4	129.4	13.557	0.856	75	75
80	3.668858	0.000016	35.6	2.0	13.283	0.034	75	75
93	3.065258	0.000002	11.4	0.3	13.255	0.009	60	75
97	2.973627	0.000000	34.2	2.2	13.104	0.034	85	85
98	2.974296	0.000070	39.4	4.1	13.135	0.080	85	85

clumpy systems. A way to investigate this issue is by observing systems which show several lines above the ADR detectability threshold and close in velocity space. If these proved to be p -type lines, we would probably be dealing with a clumpy system covering one LOS. We claim that Figure 5 argues against such a picture for the $z \approx 3.10$ system since line 7 (t) lies between lines 3 and 4 (p).

There are two main caveats concerning our results. First, the sample of lines is small and this is expected to affect the estimates themselves because it is not just the fraction of hits and misses that is important (Fang et al. 1996). The most probable size calculated reflects the LOS separation over a small redshift range. It is unclear whether the result would remain similar if a broader redshift range were covered. If such a sample were available, it would be possible to carry out size estimates in different redshift bins so as to look for any evolutionary trends in the estimated absorber sizes. Evolution of the UV background field would be expected to have an effect on absorber sizes. If these are predominantly photoionized, we might expect size estimates for C IV absorbers to become smaller at low z . Note however that apparent redshift evolution may be an artefact due to LOS separation (Fang et al. 1996; Dinshaw et al. 1998) and, therefore, difficult to confirm.

Second, the redshift of the lens is unknown; multiple lensing would introduce further complications. Thus these results only give an order of magnitude estimate of C IV absorber size.

It is worth noting that these results agree in order of magnitude, at least for the lower z_1 values, with recent results from work on a larger sample with separate spectra for different LOS (Rauch et al. 2001). These authors found that there is very little difference between column densities in separate spectra for LOS separations below about $300 h_{50}^{-1}$ pc. On the other hand, column density differences reach 50% just below LOS separations of $\sim 1 h_{50}^{-1}$ kpc. From energy arguments these authors conclude that C IV clouds are the end products of ancient galactic outflows. There is also independent evidence for such a scenario. Theuns et al.

(2002) showed that hydrodynamical simulations with feedback produce C IV absorption lines with properties in reasonable agreement with observations. They used the same Voigt profile fits to C IV lines which we have used in the present paper, together with fits to one more QSO to demonstrate this result. It is thus possible that the structures examined here represent clouds whose baryonic content has been transported, or at least metal-enriched, to large distances (up to ~ 1 Mpc) from the central regions of their parent galaxies.

Our results also agree with the results of Petitjean et al. (2000) for Mg II systems. These authors used equivalent width models in which one LOS was saturated and one optically thin to estimate that $\log N(\text{Mg II})$ for $z < 1.7$ absorbers changes by at least an order of magnitude over less than $\sim 1 h_{75}^{-1}$ kpc. However, there is no indication that the two populations may belong to the same class, as there are no low ionization lines associated to any of our C IV lines which show an ADR. Although there are some low ionization lines associated to some of the other C IV lines in the full sample, these do not show multiplets, so that it is not possible to look for evidence of partial coverage. There is also no overlap in redshift between the two populations.

On the other hand, if our somewhat higher estimates for $z_1 = 2.974$ are closer to reality, then these would support the picture according to which intervening C IV absorbers arise in PGCs (Haehnelt et al. 1996, Rauch et al. 1997).

Note that in total there are 8 (10) components which are either p or t , depending on whether we count lines 25 and 26. 4 out of these are p which is a fraction of 0.5 (0.4). Of course, this is a single case and its statistical significance cannot be estimated. However, even if, in a worst case scenario, we trust only one (observed) line, this result says that the probability of partial coverage for lines above the detectability limit is not negligible. This in turn suggests that for gravitationally lensed QSOs partial coverage by intervening structures is not rare and observing it is mainly an issue of detectability.

8 CONCLUSIONS

The spectra used in this work are the result of careful wavelength and flux calibration, and order merging. The observed ADRs are thus real, and we have shown that in many cases they can be simulated by means of a simple physical model. From LOS separations at different redshifts we obtained lower limit estimates of $\sim 300 h_{72}^{-1}$ pc for C IV absorbers. From a statistical approach we obtained most probable sizes of a few kiloparsecs, but, because the sample is small, this estimate is rather uncertain.

We have briefly discussed the possible nature of the absorbers based on our size estimates. Clearly, more work needs to be done before we can decide among different possibilities. In this respect it would be interesting to carry out a cross-correlation study between Lyman break galaxies and our C IV absorbers similar to the work by Adelberger et al. (2002) who found that the two classes may be related.

Ideally, one would like to have separate spectra for different LOS. However, given that lensed QSOs may have small image separations, it is difficult to find suitable candidates. The technique used here compensates for this problem as it allows probing of closer LOS. All that is required is the existence of two images with a known angular separation as well as an estimate for the redshift of the lens. As in the case studied here, the separation may be obtained in the course of different observations with different instruments (e.g. space based) or in different wavebands (e.g. radio) where the necessary resolution can be attained. Obtaining a reliable value for z_l is more difficult as it depends on a combination of modelling and detection of the lensing mass, but if there are several candidates, several models can be run.

In principle the method could be extended to more than two images. However, with several images of different brightnesses the uncertainties in the zero level adjustment parameter would probably allow different configurations. It may be possible to add a probability argument for these as well, but adding this degree of complexity for what would be a small sample is not likely to yield worthwhile results.

Finally, it is worth noting that ADRs can be useful in a different way as well. In cases of spectra of QSOs which are not known to be lensed, the need for same, or similar, ADR corrections for several absorbers would be a strong indication that a QSO is lensed. The method illustrated in this paper would then have to be modified to include the angular separation as an unknown as well, with more speculative results.

ACKNOWLEDGMENTS

The observations were made at the W. M. Keck Observatory, which is operated as a scientific partnership between the California Institute of Technology and the University of California; it was made possible by the generous support of the W. M. Keck Foundation.

REFERENCES

- Adelberger K.L., Steidel C.C., Shapley A.E., Pettini M., 2002, *astro-ph/0210314*
- Bechtold J., Yee H.K.C., 1995, *AJ*, 110, 1984
- Cooke A.J., 1994, PhD thesis, Univ. Cambridge
- Crotts A.P.S., Bechtold J., Fang Y., Duncan R.C., 1994, *ApJ*, 437, L79
- Dinshaw N., Foltz C.B., Impey C.D., Weymann R.J., 1998, *ApJ*, 494, 567
- Dinshaw N., Foltz C.B., Impey C.D., Weymann R.J., Morris S.L., 1995, *Nat*, 373, 223
- Dinshaw N., Weymann R.J., Impey C.D., Foltz C.B., Morris S.L., Ake T., 1997, *ApJ*, 491, 45
- D'Odorico V., Cristiani S., D'Odorico S., Fontana A., Giallongo E., Shaver P., 1998, *A&A*, 339, 678
- Downes D., Neri R., Wiklind T., Wilner D.J., Shaver P.A., 1999, *ApJ*, 513, L1
- Egami E., Neugebauer G., Soifer B.T., Matthews K., Ressler M., Becklin E.E., Murphy T.W. Jr., Dale D.A., 2000, *ApJ*, 535
- Efstathiou G., Schaye J., Theuns T., 2000, *Royal Society of London Philosophical Transactions Series*, 358, 2049
- Egami E., Neugebauer G., Soifer B.T., Matthews K., 2000, *ApJ*, 535, 561
- Ellison S.L., Lewis G.F., Pettini M., Sargent W.L.W., Chaffee F.H., Foltz C.B., Rauch M., Irwin M.J., 1999a, *PASP*, 111, 946
- Ellison S.L., Lewis G.F., Pettini M., Chaffee F.H., Irwin M.J., 1999b, *ApJ*, 520, 456
- Fang Y., Duncan R.C., Crotts A.P.S., Bechtold J., 1996, *ApJ*, 462, 77
- Foltz C.B., Weymann R.J., Röser H.-J., Chaffee F.H., 1984, *ApJ*, 281, L1
- Freedman W.L. et al., 2001, *ApJ*, 553, 47
- Griesmann U., Kling R., 2000, *ApJ*, 536, L113
- Haehnelt M.G., Steinmetz M., Rauch M., 1996, *ApJ*, 465, L95
- Hamann F., Ferland G., 1999, *ARA&A*, 37, 487
- Hogg D.W., 2000, *astro-ph/9905116*
- Ibata R.A., Lewis G.F., Irwin M.J., Lehár J., Totten E.J., 1999, *AJ*, 118, 1922
- Irwin M.J., Ibata R.A., Lewis G.F., Totten E.J., 1998, *ApJ*, 505, 529
- Kobayashi N., Terada H., Goto M., Tokunaga A., 2002, *ApJ*, 569, 676
- Lewis G.F., Ibata R.A., Ellison S.L., Aracil B., Petitjean P., Pettini M., Srianand R., 2002, *MNRAS*, 334, L7
- Loh J.-M., Quashnock J.M., Stein M.L., 2001, *ApJ*, 560, 606
- Lopez S., Hagen H.-J., Reimers D., 2000, *A&A*, 357, 37
- McGill C., 1990, *MNRAS*, 242, 544
- Mo H.J., Miralda-Escudé J., 1996, *ApJ*, 469, 589
- Monier E.M., Turnshek D.A., Lupie O.L., 1998, *ApJ*, 496, 177
- Peebles P.J.E., 1993, *Principles of Physical Cosmology*. Princeton Univ. Press, Princeton
- Perlmutter S. et al., 1999, *ApJ*, 517, 565
- Petitjean P., Aracil B., Srianand R., Ibata R., 2000, *A&A*, 359, 457
- Petitjean P., Bergeron J., 1994, *A&A*, 283, 759
- Petitjean P., Surdej J., Smette A., Shaver P., Mückelt J., Remy M., 1998, *A&A*, 334, L45
- Rauch M., 1998, *ARA&A*, 36, 267
- Rauch M., Haehnelt M.G., Steinmetz M., 1997, *ApJ*, 481, 601
- Rauch M., Sargent W.L.W., Barlow T.A., 1999, *ApJ*, 515, 500
- Rauch M., Sargent W.L.W., Barlow T.A., 2001, *ApJ*, 554, 823
- Rauch M., Sargent W.L.W., Womble, D.S., Barlow T.A., 1996, *ApJ*, 467, L5
- Riess et al., 2001, *ApJ*, 560, 49
- Riess et al., 1998, *AJ*, 116, 1009
- Rigby J.R., Charlton J.C., Churchill C.W., 2002, *ApJ*, 565, 743
- Sargent W.L.W., Boksenberg A., Steidel C.C., 1988, *ApJS*, 68, 539
- Sargent W.L.W., Young P.J., Boksenberg A., Carswell R.F., Whelan J.A.J., 1979, *ApJ*, 230, 49
- Shaver P.A., Robertson J.G., 1983, *ApJ*, 268, L57

- Smette A., Surdej J., Shaver P.A., Foltz C.B., Chaffee F.H., Weymann R.J., Williams R.E., Magain P., 1992, *ApJ*, 389, 39
- Smette A., Robertson J.G., Shaver P.A., Reimers D., Wisotzki L., Köhler Th., 1995, *A&AS*, 113, 199
- Steidel C.C., 1993, in Majewski S.R., ed., *ASP Conf. Ser. Vol. 49, Galaxy Evolution: The Milky Way Perspective*. Astron. Soc. Pac., San Francisco, p. 227
- Theuns T., Viel M., Kay S., Schaye J., Carswell R.F., Tzanavaris P., 2002, *ApJ*, 578, L5
- Webb J. K., 1987, PhD thesis, Univ. Cambridge
- Young P.A., Impey C.D., Foltz C.B., 2001, *ApJ*, 549, 76
- Young P., Sargent W.L.W., Boksenberg A., Oke J.B., 1981, *ApJ*, 249, 415